Effects of the Zhang-Li Torque on Magnetic Droplet Solitons

Author: Jan Albert Iglesias
Advisor: Joan Manel Hernàndez Ferràs
Facultat de Física, Universitat de Barcelona, Diagonal 645, 08028 Barcelona, Spain.

Abstract: Spin-transfer nano-oscillators are devices in which spin-transfer torques can generate localized spin waves (dissipative solitons) called magnetic droplet solitons. We have studied the specific effects of the Zhang-Li torque on these solitons. To do so, we have analytically solved for an accurate electric current distribution and its Oersted fields and we have then used `mumax`[3] to get the evolution of the magnetization. We have found that this torque either enlarges or shrinks droplets and also raises or lowers generation current thresholds depending on the configuration of the device. In addition, we have eventually outlined a method for controlling the relative impact of this torque.

I. INTRODUCTION

Magnetic oscillators are becoming a popular field of study given their potential applications in electronics. In particular, spin-transfer nano-oscillators (STNOs), which are nanoscale magnetic oscillators driven by spin-polarized currents, are promising devices. They are comprised of two ferromagnetic layers separated by a non-magnetic conducting material set between two electric contacts (the nanocontact (NC) and the large contact (LC)), as shown in Fig. 1. One of the two magnetic layers, the polarizer layer (PL), is thick enough to maintain its magnetization constant. Whereas the magnetization of the thinnest one, the free layer (FL), changes easily.

When an electric current is applied through the contacts (note that all mentioned layers are conducting), conduction electrons align their spin with the PL's magnetization $\vec{m}_p$, and the current becomes spin-polarized. Then, through what is known as spin-transfer torque effect, this current might modify and even reverse the magnetization of the FL in a region just beneath the nanocontact, generating what is called a magnetic droplet soliton (MDS) [1]. This is nothing but a stable state of reversed magnetization that oscillates at a specific frequency. What makes STNOs so versatile is the fact that this frequency can be controlled by the electric current and the magnetic field $\vec{B}$ we apply to them.

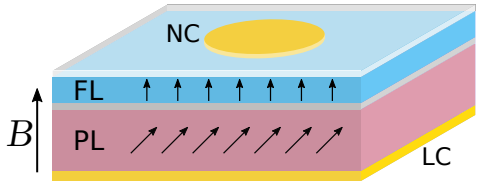

FIG. 1: Schematic representation of a STNO.

Many authors have thoroughly analysed MDSs by means of micromagnetic simulations to determine interesting features such as threshold currents at which they are generated/annihilated, oscillating frequencies and sizes. However, most of them assumed the applied current followed a uniform vertical distribution that led to a cancellation of the Zhang-Li torque, as will be discussed in subsequent sections. Recent studies [2] have observed MDSs being larger than expected, and the authors claimed the origin could be in the Zhang-Li torque. Hence, we have accurately simulated the dynamics of the FL's magnetization to study the effects of this torque and test their claim. We have also looked for any other relevant effects of this torque.

II. MAGNETIZATION DYNAMICS

The reduced magnetization $\vec{m}$ (dimensionless) of the FL obeys the following dynamical equation [3][4].

$$\frac{\partial \vec{m}(\vec{r},t)}{\partial t} = \vec{\tau}_{\mathrm{LL}} + \vec{\tau}_{\mathrm{SL}} + \vec{\tau}_{\mathrm{ZL}}, \tag{1}$$

where the three terms on the right hand side are the Landau-Lifshitz (LL), Slonczewski (SL) and Zhang-Li (ZL) torques respectively.

1. Landau-Lifshitz torque This torque accounts for the interaction between the magnetization and an effective magnetic field $\vec{B}_{\mathrm{eff}}$ that contains external, demagnetizing and exchange fields among others. In one of its forms, it can be written as

$$\vec{\tau}_{\mathrm{LL}} = -\gamma \frac{1}{1+\alpha^2}\left[\vec{m}\times\vec{B}_{\mathrm{eff}} + \alpha\left(\vec{m}\times\left(\vec{m}\times\vec{B}_{\mathrm{eff}}\right)\right)\right], \tag{2}$$

where γ is the gyromagnetic ratio and α is the damping parameter. As shown in Fig. 2(a), the first term results in a vector that is perpendicular both to $\vec{m}$ and $\vec{B}_{\mathrm{eff}}$, forcing $\vec{m}$ to undergo precession around $\vec{B}_{\mathrm{eff}}$. The second term points to the precession center, reducing the precession radius and aligning $\vec{m}$ with $\vec{B}_{\mathrm{eff}}$. It is thus the damping term; and its effectiveness depends on α.

2. Slonczewski spin-transfer torque Spin-transfer torques (namely SL and ZL) may become nonzero when a spin-polarized electric current goes through the FL. In the studied device, the SL torque reads

$$\vec{\tau}_{\mathrm{SL}} = \gamma \frac{j_z \hbar}{e M_{\mathrm{sat}} d} \frac{\epsilon}{1+\alpha^2}\left[\vec{m}\times\left(\vec{m}_p\times\vec{m}\right)+\alpha\left(\vec{m}\times\vec{m}_p\right)\right], \tag{3}$$

where j_z is the vertical current density, $\vec{m}_p$ is the PL's magnetization (which is constant) and ϵ is a factor that

is proportional to the spin-polarization P of the current. Remaining parameters are either universal constants or are related to the geometry and materials of the device.

The first term of Eq. (3) can be responsible for MDSs generation by counteracting the LL damping term. Take the system described in Fig. 1 initially with an external magnetic field $\vec{B}$ pointing upwards and without any applied current. The initial FL's $\vec{m}$ would be pointing upwards. If a downward ($j_z < 0$) spin-polarized current goes then through the FL, the first term of the SL torque opposes the LL damping term. Wherever the current is high enough, $\vec{m}$ reverses and the MDS is generated. Fig. 2(b) depicts this situation. Note that this can only be achieved if the FL has vertical uniaxial anisotropy, making the reversed state stable enough to become a soliton. Then, the only relevant component of $\vec{m}_p$ is the z one. The second term of Eq. (3) just modulates the precession term of the LL torque (first term of Eq. (2)).

3. Zhang-Li spin-transfer torque In a first order approximation the spin-transfer effect can be considered adiabatic. Then, the torque added by Zhang and Li becomes

$$\vec{\tau}_{\mathrm{ZL}} = -\gamma \frac{\hbar}{2eM_{\mathrm{sat}}} \frac{1}{1+\alpha^2} \Big[\vec{m}\times\big(\vec{m}\times(\vec{\jmath}\cdot\vec{\nabla})\vec{m}\big) - \alpha\,\big(\vec{m}\times(\vec{\jmath}\cdot\vec{\nabla})\vec{m}\big)\Big], \quad (4)$$

where $\vec{\jmath}$ is the electric current density. The FL is thin enough to neglect derivatives in z, and the symmetry of the system will lead to $j_\theta = 0$, as will be discussed in the following section. Then, $\vec{\jmath}\cdot\vec{\nabla} = j_\rho \frac{\partial}{\partial \rho}$ (in cylindrical coordinates (ρ, θ, z)) and the radial direction is enough to study the ZL effects.

Fig. 2(c) depicts the first term of Eq. (4) for a set of magnetic moments reversing along the radial direction ρ. It represents a section of a downwards-pointing MDS in an upward surrounding (where $\rho = 0$ would be the MDS's center). This figure corresponds to the $j_\rho > 0$ case, which we have called ZL− (because it will imply $j_z < 0$). One can see τ_1 opposes droplet formation since it favors upwards-pointing magnetic moments near the domain wall. In the opposite case (i.e. ZL+, for which $j_\rho < 0$) $\vec{\tau}_1$ would be reversed, favoring MDS generation. The second term of Eq. (4) is perpendicular to the first one hence it causes $\vec{m}$ to move in the angular direction, but it will not be relevant in subsequent discussions.

Notice that j_ρ needs to be nonzero for the ZL torque to have an impact on MDSs. It is for this reason that simulations that consider completely vertical uniform currents show no traces of this torque. One must use a more accurate current distribution to spot ZL effects.

We have solved Eq. (1) using a micromagnetic simulation software named `mumax`[3] [3]. However, we had to provide it with the applied electric current distribution and corresponding Oersted fields. So let us compute both for the given system.

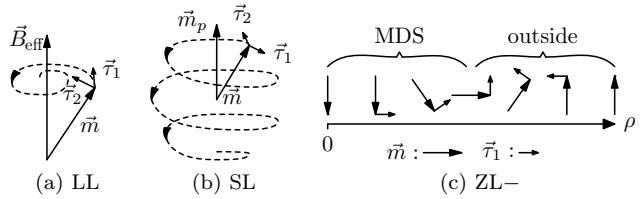

(a) LL (b) SL (c) ZL−

FIG. 2: Directions of the different torques. $\vec{\tau}_1, \vec{\tau}_2$ represent the first and second terms of each torque respectively.

III. ELECTRIC CURRENT DISTRIBUTION

Although the system is composed of several conducting layers, we will take the approximation of a single-layer device to allow for analytical solutions. This approximation is reasonable because metals generally have similar resistivities. Additionally, we will neglect the Hall effect produced by the applied magnetic field $\vec{B}$. Therefore, the system gets simplified to what is shown in Fig. 3, an infinite metallic layer set between two electrical contacts with cylindrical symmetry.

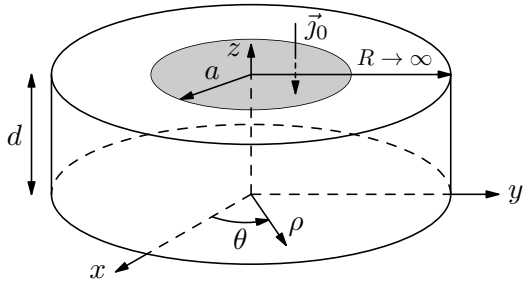

FIG. 3: Simplified geometry of a STNO.

In ohmic materials [5] the electric field $\vec{E}$ and the current density $\vec{\jmath}$ are related by $\vec{E} = \varrho\vec{\jmath}$, where ϱ is the material's resistivity. $\vec{\jmath}$ can be rewritten in terms of the electric potential V (using $\vec{E} = -\vec{\nabla}V$),

$$\vec{\jmath} = -\frac{1}{\varrho}\vec{\nabla}V. \quad (5)$$

Additionally, since electric charge is always conserved, the current density must satisfy the continuity equation $\frac{\partial \rho}{\partial t} + \vec{\nabla}\vec{\jmath} = 0$, where ρ is the electric charge density. Assuming now the stationary limit is quickly reached, the partial derivative with respect to time can be neglected leaving $\vec{\nabla}\vec{\jmath} = 0 \Rightarrow \vec{\nabla}\frac{\vec{\nabla}V}{\varrho} = 0$.

Since the system is now composed of a single ideal ohmic material, ϱ is constant and nonzero, so it commutes with the nabla operator and it can be dismissed. Therefore, the equation that describes the electric current density in the system is nothing but Laplace's equation for the electric potential,

$$\nabla^2 V = 0. \quad (6)$$

Given the symmetry of the system, it is convenient to work in a cylindrical coordinate system (ρ, θ, z). Then, by using the separation of variables method [6] and assuming V does not depend on θ, one gets the general solution

$$V(\rho, z) = (C_1 \sinh(kz) + C_2 \cosh(kz))(J_0(k\rho) + C_3 N_0(k\rho)).$$

Where C_1, C_2, C_3 and k are constants to be determined by boundary conditions and J_0 and N_0 are the 0th order Bessel functions of first and second kind respectively.

The boundary conditions (BCs) of this ideal system are those of a material connected by perfect electrical contacts, namely

(i) $V(\rho, z) < \infty \quad \rho \to 0$
(ii) $V(\rho, z = 0) = 0$
(iii) $V(\rho, z) = 0 \quad \rho \to \infty$
(iv) $j_z(\rho, z = d) = j_0\, \theta(a - \rho)$.

BC (i) results from requiring the electric potential to be finite everywhere, especially at the center of the system. This BC accounts for the fact that energy cannot diverge and it implies $C_3 = 0$.

BC (ii) sets the zero of the electric potential at the bottom of the device, where the large ideal electrode is placed. Applying this BC leads to $C_2 = 0$.

BC (iii) sets the zero of V at infinity in the radial direction, implicitly stating that the radial width of the system is very large compared to its height. In a finite system, this BC would restrict the possible values of k by a relation with the discrete roots of Bessel functions. However, since the boundary is sent to infinity, such a restriction does not appear and k becomes a continuous variable. The most general solution is then the sum (actually an integration) for all possible values of k.

$$V(\rho, z) = \int_0^\infty C_1(k) \sinh(kz) J_0(k\rho)\, dk.$$

To determine $C_1(k)$ one needs to use BC (iv), which describes our control of the device. More precisely, it states that a given uniform current j_0 enters the cylinder through a nanocontact of radius a placed at $z = d$. By using Eq. (5) and the orthonormality relation of Bessel functions $\int_0^\infty J_0(k\rho) J_0(k'\rho)\, \rho\, d\rho = \frac{1}{k}\delta(k - k')$ [6], one gets an expression for $C_1(k)$ that leads to the solution

$$V(\rho, z) = -\varrho\, j_0\, a \int_0^\infty \frac{\sinh(kz) J_1(ka) J_0(k\rho)}{k \cosh(kd)}\, dk. \qquad (7)$$

To get the electric current density $\vec{j}$ one just needs to plug Eq. (7) into Eq. (5). Note that $j_\theta = 0$ because V does not depend on θ. Fig. 4 shows electric current field lines for a case with $a = d = 100\,\text{nm}$. Note how the distribution is far from the uniform case and that the FL (a sheet of differential thickness placed at a height $h = 92\,\text{nm}$) experiences $j_\rho \neq 0$.

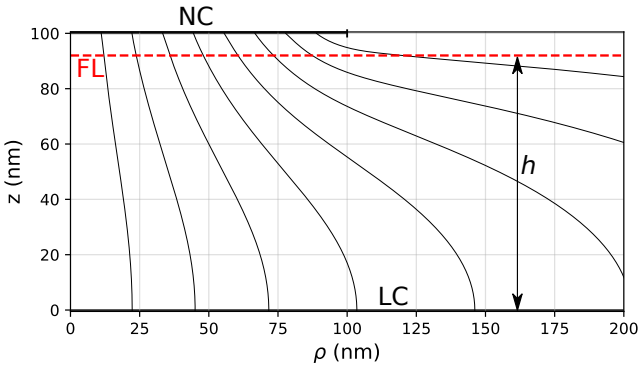

FIG. 4: Electric current streamlines in a vertical section. The dashed red line marks the FL's position. NC and LC denote the nanocontact and the large contact respectively.

IV. OERSTED FIELDS

According to the Biot–Savart law (BS law) [5], electric currents generate magnetic fields that are usually called Oersted fields. Since we are studying magnetic properties, these fields ought not to be overlooked, so let us compute those generated by our current distribution.

Given the symmetry of the system, the magnetic field will only have a nonzero component in the azimuthal direction. To see this, one can compute the cross product of $\vec{j}$ and a position vector $\vec{l}$ (i.e. part of the integrand in the BS law),

$$\vec{j} \times \vec{l} = \begin{vmatrix} \vec{a_\rho} & \vec{a_\theta} & \vec{a_z} \\ j_\rho & 0 & j_z \\ l_\rho & l_\theta & l_z \end{vmatrix} = -l_\theta j_z \vec{a_\rho} + (l_\rho j_z - l_z j_\rho)\vec{a_\theta} + l_\theta j_\rho \vec{a_z}.$$

Two volume elements located at (ρ, θ, z) and $(\rho, -\theta, z)$ would have exactly the same properties except for the corresponding values of l_θ, which would have opposite signs. Therefore, once integrated over all space, only the azimuthal component of the cross product would survive.

Knowing now the direction of the magnetic field, one can take an approach that is much simpler than the BS law; Ampère's law [5]. By taking a coaxial hoop of radius ρ as the closed circuit, one gets a simple expression for the generated magnetic field.

$$\vec{B} = \frac{\mu_0}{\rho} \int_0^\rho j_z\, \rho'\, d\rho'\ \vec{a_\theta}. \qquad (8)$$

This expression only depends on the z component of the interior current, and it is computed by a simple integration rather than the 3-variable integration of the BS law. Therefore, the current density and the magnetic field need not be computed outside the FL saving, thus, much computing time. Both expressions are now simple enough to be quickly evaluated using numerical integration methods.

V. SIMULATIONS

We have modelled the FL as a 1-cell-thick 256×256 grid of cell size $c = 4\,\text{nm}$ placed at a distance h from the LC. Then, we have developed an assisting `python` program to evaluate the analytical expressions of Eq. (7) and Eq. (8) at each point of the grid and generate arrays with the current density and its Oersted fields. With these vector fields as inputs, we have used `mumax`^{3} to solve Eq. (1). This software groups all contributions in $\vec{B}_{\text{eff}}$ and obtains the time evolution of the FL's magnetization $\vec{m}$ using finite differences methods [3].

The parameters we have used in our simulations are similar to those of the experimental devices used by Hang *et al.* [7] in order to give an accurate description of real devices. It is for this reason that we have chosen $a = 100\,\text{nm}$, $P = 0.5$, $\vec{B} = (0, 0, 0.5)\,\text{T}$, $M_{\text{sat}} = 500\,\text{kA/m}$ and $\alpha = 0.03$. We have also considered the FL to have in-plane periodic boundary conditions and vertical uniaxial anisotropy with constants $K_1 = 200\,\text{kJ/m}^3$ and $K_2 = 0$. Our simulations took off from an initial state with $\vec{m}$ forming an angle of 2^o with the vertical in order for it to start moving.

As for the PL, recall it is thick enough to consider its magnetization constant, so its dynamics need not be studied. We have taken $\vec{m}_p = (\frac{1}{\sqrt{2}}, 0, \frac{1}{\sqrt{2}})$, which is reasonable for a usual case of a permalloy (Ni 80% Fe 20%) PL with an applied 0.5 T vertical magnetic field.

VI. RESULTS

A. Zhang-Li torque effects

We have simulated the droplet generation process by applying upward current sweeps to the system (i.e. slowly increasing currents starting from zero). In order to spot the specific effects of the ZL torque, we have done so in three different configurations; one with $j_z > 0$, $(m_p)_z < 0$ (ZL+), another with $j_z < 0$, $(m_p)_z > 0$ (ZL−) and a latter disabling the ZL torque (no-ZL). In this way, the LL and SL torques are identical in all cases and only the ZL torque differs.

We have used one of the outputs of `mumax`^{3}, the total magnetization $\vec{M}$, to estimate the droplet's area using the relation $A_{\text{MDS}} = \frac{A_{\text{total}}(1-M_z)}{2}$, which results from considering that the MDS has $m_z = -1$ and completely opposes its surroundings. We have then obtained an effective radius by thinking of MDSs as circular, an approximation that holds quite well at these current densities. Fig. 5 shows our results.

The first relevant fact is that the three curves show a threshold current at which the droplet is generated. This is in agreement with the general behaviour seen in experiments [7] and simulations [8] carried out by other authors. But our simulations are novel in that they allow us to go further and discern the ZL torque.

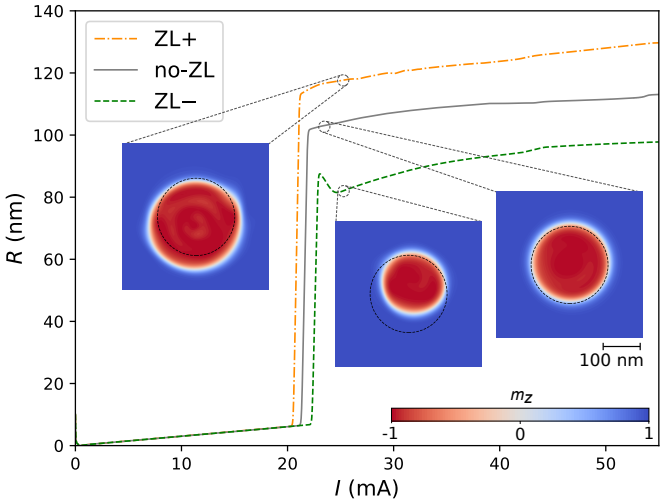

FIG. 5: Estimated droplet radius *vs* applied current at the nanocontact for upward current sweeps with different ZL torques. Insets show m_z of the FL (the dashed black line denotes the NC). These simulations were carried out taking $a = h = 100\,\text{nm}$, $d = 108\,\text{nm}$.

One can point out two main differences between the curves in Fig. 5; droplet radii once formed and generation current thresholds. As far as radii are concerned, ZL+ results in a radius increase while ZL− shows a decrease compared to the no-ZL case. This behaviour can be cross-checked with insets of Fig. 5, which show MDSs as seen from above. These results seem, indeed, to back Chung *et al.*'s [2] conclusion that the experimental radius increase they found was caused by the ZL torque. Nevertheless, this is not entirely conclusive since other effects such as stochastic drift instabilities could also account for it.

As for current thresholds, we have found ZL+ to reduce the generation current and ZL− to increase it, as compared to the no-ZL case. This fact has not been pointed out before and we believe it might be quite relevant in technology. It implies that, depending on the orientation of the PL and the electric current, the required intensity to generate MDSs can be lowered some mA.

Both effects can be qualitatively explained with the discussion in section II.3. As Fig. 2(c) shows, ZL− favors upward moments near the domain wall, obstructing droplet formation. Thus, it reduces their radii and more energy (i.e. larger currents) is required to form them. Analogously, ZL+ helps in droplet formation, so it enlarges droplets and lowers thresholds.

B. Controlling the ZL torque

To exploit the discussed effects, we have studied systems with different 'strengths' of the ZL torque. In the present device, this torque is proportional to the in-plane current density, which can be controlled by the device's height d. That is, a thin layer would have an almost uni-

form current distribution (i.e. with a small in-plane component) while a thicker one would lead to more spread-out currents (as that of Fig. 4), with a saturation at the $d \to \infty$ limit. What we are suggesting is that by changing the device's z-thickness we would be able to modulate the ZL torque. Experimentally, this could be achieved, for instance, by changing the PL's thickness.

We have conducted simulations for different device heights keeping the FL at the same 8 nm distance to the top and changing the distance between the FL and the bottom contact h for the no-ZL, ZL+ and ZL− cases. We have obtained a figure similar to Fig. 5 for each h, and we summarize our results in Fig. 6.

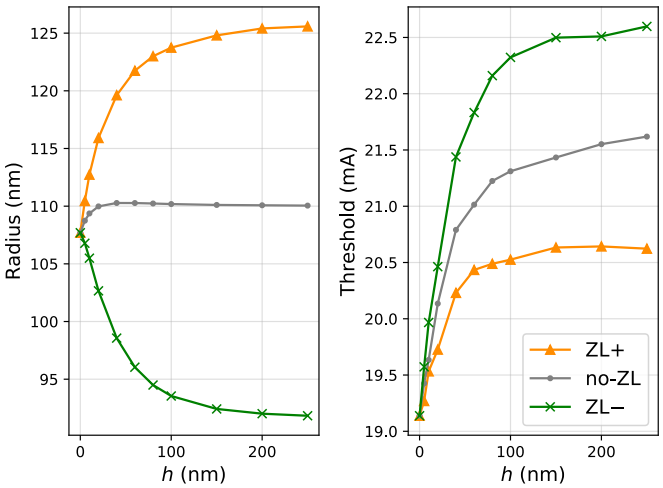

FIG. 6: Left: Estimated droplet radius at a representative current of $I = 40\,\text{mA}$ *vs* h. Right: Generation current threshold *vs* h. These simulations were carried out taking $a = 100\,\text{nm}$, $d = h + 8\,\text{nm}$. Connecting lines are merely meant to be a guide to the eye.

As we have discussed, the radius is increased by ZL+ and decreased by ZL−, as compared to the no-ZL case (for which the radius merely changes with h). We can also see these effects become more important as h is increased, reaching a saturation that corresponds to the current distribution saturation for $d \to \infty$.

Similarly, current thresholds show the discussed effects. It is not surprising that the current threshold depends on h *also* in the no-ZL case. This fact is due to charge conservation; when h is raised, the current distribution spreads out and j_ρ increases at expenses of j_z. Thus, $|j_z|$ decreases, reducing the SL torque and increasing the necessary applied current to reverse $\vec{m}$ and generate the droplet. It is for this reason that thresholds increase with h in all cases. But the ZL+ torque counteracts this fact and leads to smaller threshold increments whereas the ZL− torque further increases them. In this case the $d \to \infty$ saturation is also reached.

VII. CONCLUSIONS

We have obtained accurate analytical expressions for the current density and Oersted fields in STNOs and we have successfully implemented them in a 2D grid (FL) by means of `python` scripts. We have also combined these arrays with a cutting-edge micromagnetic simulation software (`mumax`[3]) and we have found previously unknown features of MDSs.

First, we have checked the ZL torque enlarges or shrinks droplets depending on how we orientate the polarizer and the applied current as Chung *et al.* have claimed [2]. Namely, when the PL points against $\vec{B}$ and $\vec{j}$ (ZL+), MDSs get bigger, whereas when the PL and $\vec{j}$ are turned over (ZL−), MDSs become smaller. Second, we have seen the ZL torque to have an impact on current generation thresholds, something that had not been reported before. Specifically, the ZL+ torque reduces generation thresholds while ZL− increases them.

We have eventually suggested a way of controlling the ZL torque that consists in changing the device's thickness. With it, we have shown one could get differences of as much as 2 mA —a significant amount in nanoelectronics— in threshold currents. Additionally, the tools we have developed enable us to easily proceed with further studies in droplet dynamics that could involve but are not limited to hysteresis of droplet generation, droplet shapes and even drift instabilities.

Acknowledgments

I would like to thank my advisor Joan Manel Hernàndez and his colleague Ferran Macià for their invaluable help as well as my wife Alba for her support.

[1] Mohseni, S.M. *et al.* "Spin Torque-Generated Magnetic Droplet Solitons". Science **339:** 6125 (2013).
[2] Chung, S. *et al.* "Direct Observation of Zhang-Li Torque Expansion of Magnetic Droplet Solitons". Phys. Rev. Lett. **120:** 217204 (2018).
[3] Vansteenkiste, A. *et al.* "The Design and Verification of MuMax3". AIP Adv. **4:** 107133 (2014).
[4] J. Stöhr, H.C. Siegmann, *Magnetism: From Fundamentals to Nanoscale Dynamics*, (Springer, Berlin 2006).
[5] D.J. Griffiths, *Introduction to Electrodynamics*, (Prentice Hall, Upper Saddle River 1999, 3rd ed.).
[6] G.B. Arfken, H.J. Weber, *Mathematical Methods for Physicists*, (Elsevier, San Diego 2005, 6th ed.).
[7] Hang, J. *et al.* "Generation and Annihilation time of Magnetic Droplet Solitons". Sci. Rep. **8:** 6847 (2018).
[8] Statuto, N. *et al.* "Generation and Stability of Dynamical Skyrmions and Droplet Solitons". Nanotechnology **29:** 325302 (2018).